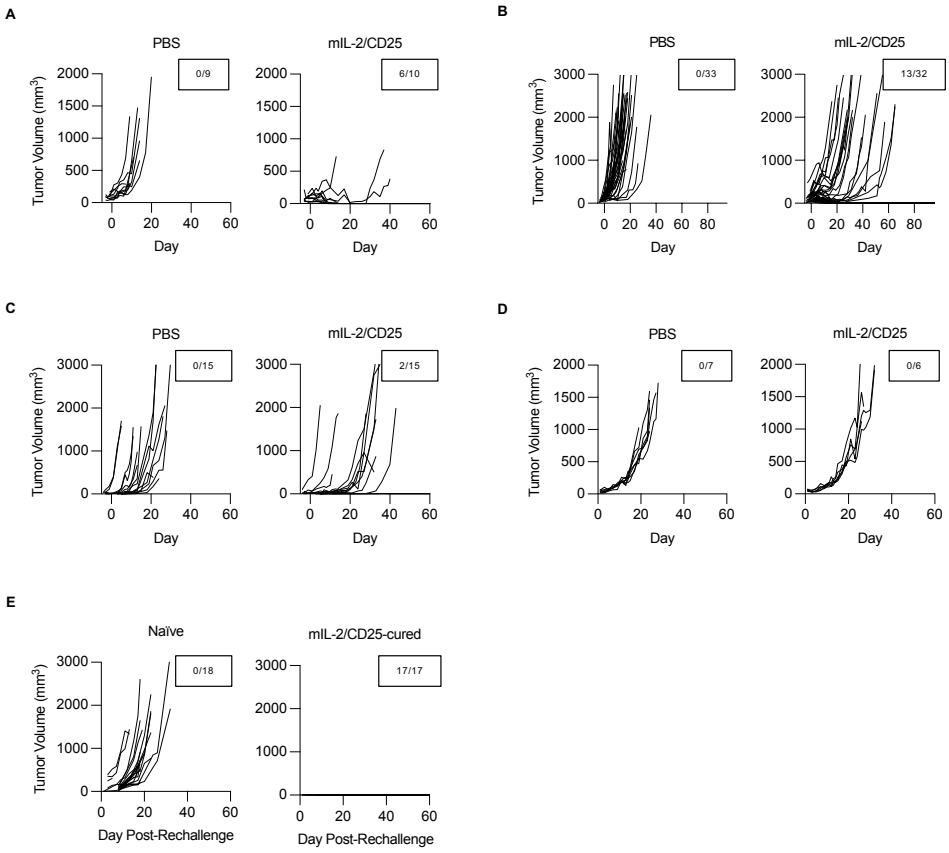

Fig. S1. HD mIL-2/CD25 delays tumor growth in immunogenic tumor models. (**A-E**) Animals were inoculated with tumors and treated as described in Fig. 1. Tumor growth curves are shown for individual animals treated with either PBS (left) or mIL-2/CD25 (right) in the (**A**) MC38 model, (**B**) CT26 model, (**C**) B16.F10 model, and (**D**) 4T1 model. (**E**) Rechallenge experiments were performed as described in Fig. 1 and tumor growth curves are shown. For all tumor growth curves, the number of surviving mice out of the total is shown. MC38 data (n=9-10/group) were pooled from 2 independent experiments. CT26 data (n=32-33/group) were pooled from 5 independent experiments. B16.F10 data (n=15/group) were pooled from 3 independent experiments. 4T1 data (n=6-7/group) were pooled from 2 independent experiments. CT26 rechallenge data (n=17-18/group) were pooled from 4 independent experiments.

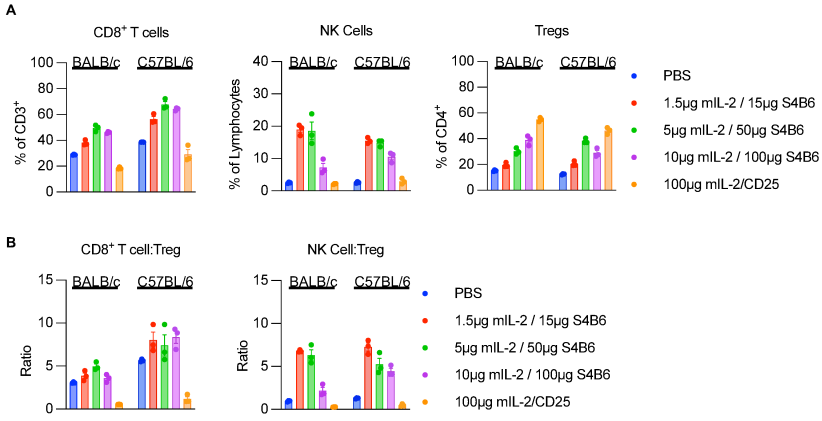

Fig. S2. The effects of different doses of S4B6-IL2/IC on CD8⁺ T cells, Tregs, and NK cells. (**A**) BALB/c and C57BL/6 mice were injected i.p. with various doses of IL-2 complexed with anti-IL-2 clone S4B6, as indicated, compared to PBS and 100 µg mIL-2/CD25. Animals were euthanized 72 hours post-injection and splenocytes were analyzed by flow cytometry. Data shows frequencies of CD8⁺ T cells, NK cells, and Tregs in both strains. (**B**) CD8⁺ T cell to Treg ratios and NK cell to Treg ratios from this experiment are shown. NK cells were defined by $CD3^{-}CD11b^{+}Ly6G^{-}CD49b^{+}$ in BALB/c mice and $CD3^{-}NK1.1^{+}$ in C57BL/6 mice. Data (n=3/group) are representative of 1 experiment. Error bars represent mean ± SD.

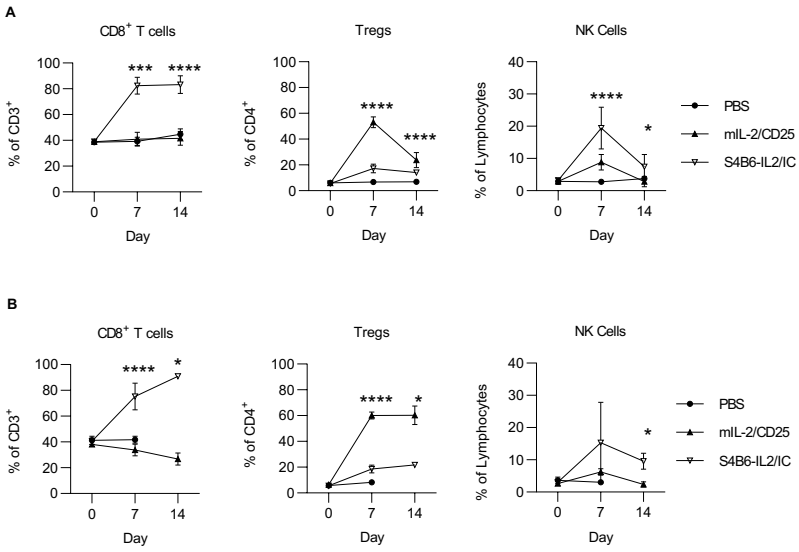

Fig. S3. Expansion of IL-2-targeted cells in the MC38 and B16.F10 models. Tumor-bearing C57BL/6 animals were treated as described in Fig. 2. (**A**) Frequencies of CD8+ T cells, Tregs, and NK cells are shown for PBMCs collected from MC38-bearing mice. (**B**) Frequencies of CD8+ T cells, Tregs, and NK cells are shown for PBMCs collected from B16.F10-bearing mice. Blood data for MC38 (n=5-9/group) and B16.F10 (n=7-8/group) were each pooled from 2 independent experiments and analyzed at each timepoint via Kruskal-Wallis test multiple comparison test. Error bars represent mean ± SD.

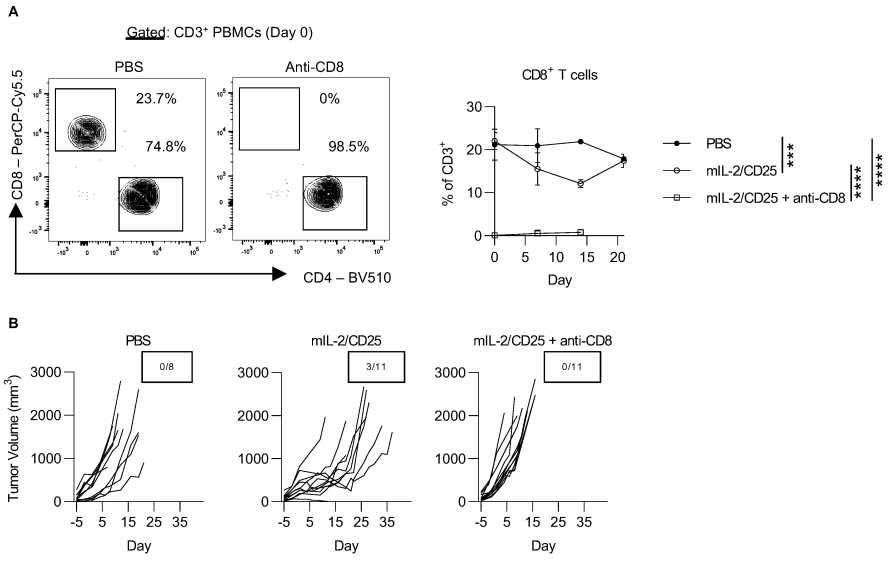

Fig. S4. CD8⁺ T cell depletion inhibits the mIL-2/CD25-induced antitumor response. CT26-bearing BALB/c mice were depleted of T cells and treated as described in Fig. 1. PBMCs were collected before, during, and after treatment in order to verify depletion by flow cytometry. (**A**) Data shows representative flow plots of $CD4^+$ and $CD8^+$ T cells after gating on $CD3^+$ T cells in the PBMCs collected on D0. The frequency of $CD8^+$ T cells of the $CD3^+$ T cell population is quantified in the blood over time. Data (n=8/11/group) were analyzed via one-way ANOVA with Tukey's multiple comparison test of the AUC. Error bars represent mean ± SD. (**B**) Tumor curves are shown for the depletion experiments.

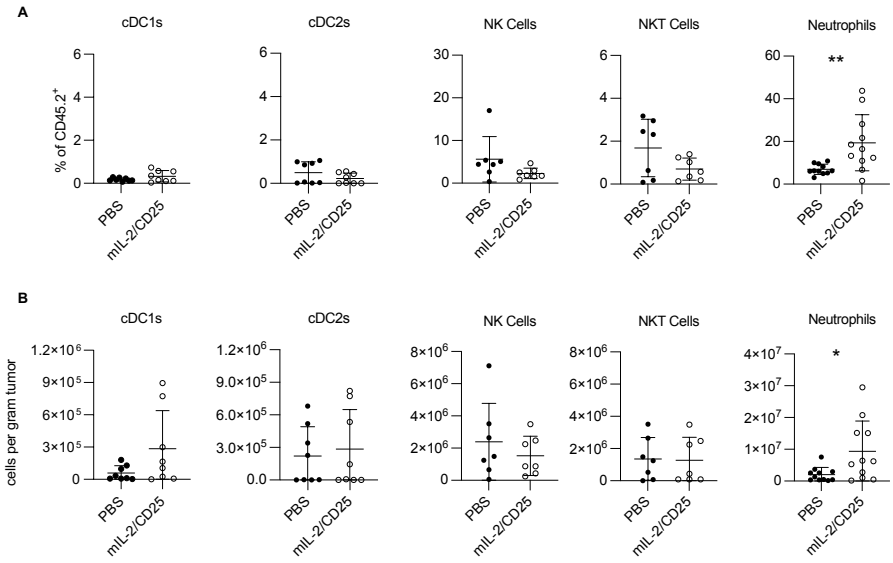

Fig. S5. The antitumor effects of mIL-2/CD25 do not act significantly through the non-T cell compartment. (**A-B**) The CT26 TME was analyzed as described in Fig. 3. Frequencies (**A**) out of the total tumor-associated immune population ($CD45.2^+$) and cell numbers per gram tumor (**B**) are shown. Type 1 conventional dendritic cells (cDC1s) were defined as live $CD45.2^+CD11b^-CD11c^+MHC\ CII^+CD8^+CD4^-$ cells. Type 2 conventional dendritic cells (cDC2s) were defined as live $CD45.2^+CD11b^-CD11c^+MHC\ CII^+CD8^-CD4^+$ cells. NK cells were defined as live $CD45.2^+CD3^-CD11b^+Ly6G^-CD49b^+$ cells. NKT cells were defined as live $CD45.2^+CD3^+CD11b^+Ly6G^-CD49b^+$ cells. Neutrophils are defined as live $CD45.2^+CD3^-CD11b^+Ly6G^+CD49b^-$ cells. Data (n=7-11/group) were pooled from 3 experiments and analyzed by Mann-Whitney test. Error bars represent mean ± SD.

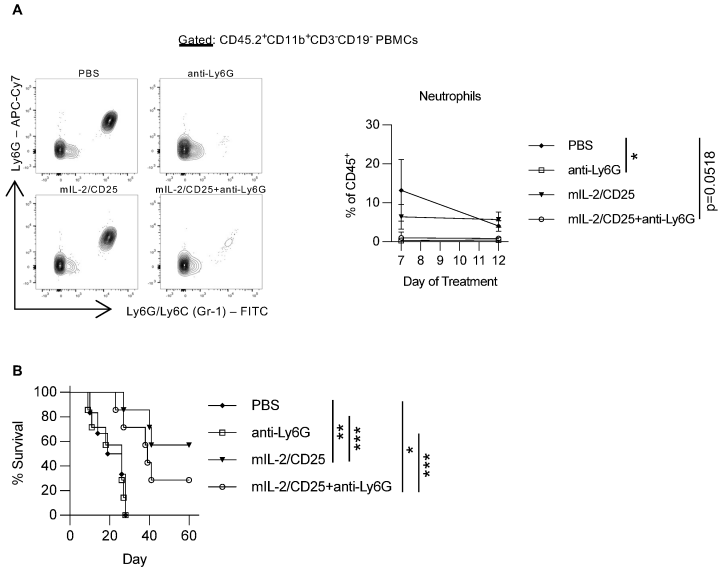

Fig. S6. Verification of Neutrophil depletion during therapy. CT26-bearing animals were depleted of Neutrophils via anti-Ly6G clone 1A8 throughout therapy. (**A**) Representative flow plots show both Ly6G and Gr-1 staining of PBMCs collected on D7 and the frequency of Neutrophils ($Ly6G^+CD11b^+CD3^-CD19^-$) of the $CD45.2^+$ immune compartment is shown for D7 and D12 PBMCs. (**B**) Mouse survival is shown. Data (n=6-7/group) were pooled from 2 independent experiments. Blood data (n=5-7/group) was analyzed as a one-way ANOVA with Tukey's multiple comparison test of the AUC. Survival data were analyzed via a Log Rank test. Error bars represent mean ± SD.

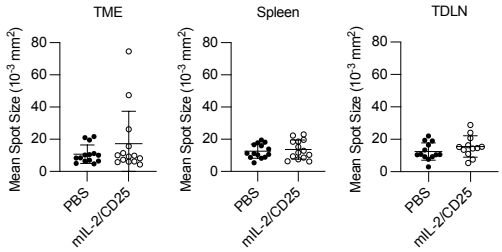

Fig. S7. HD mIL-2/CD25 does not increase the levels of IFNγ made on a per CD8$^+$ T cellular basis. Mean spot size is shown for the IFNγ ELISpot experiments from Fig. 5. ELISpot data (n=12-14/group) were pooled from 5 independent experiments and analyzed by Mann-Whitney test. Error bars represent mean ± SD.

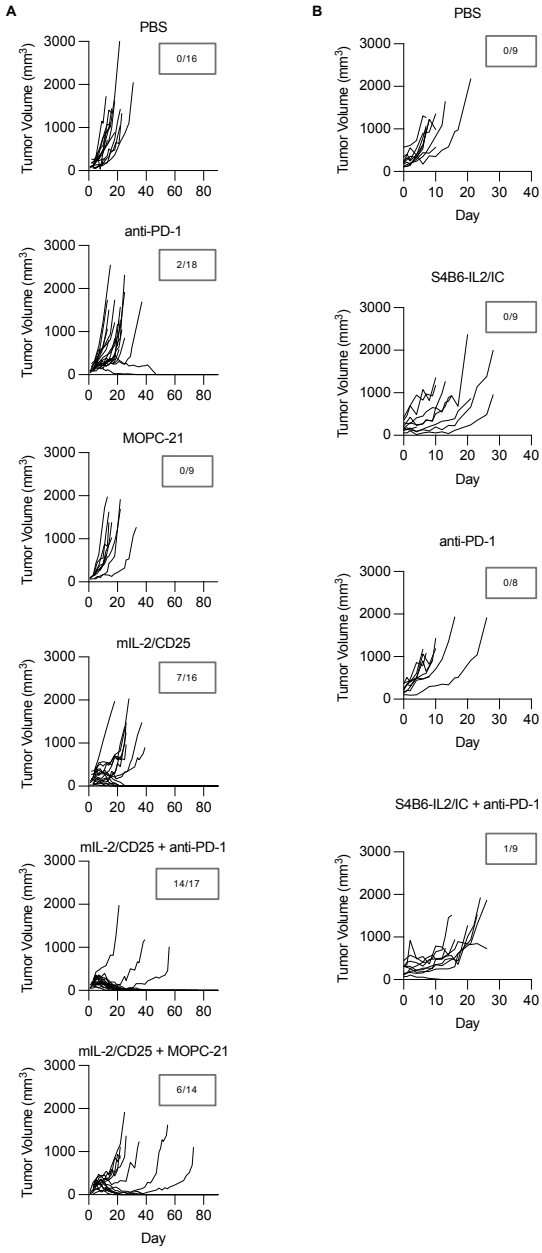

Fig. S8. HD mIL-2/CD25 combined with PD-1 blockade supports higher inhibition of tumor progression. (**A**) Tumor growth is shown for the mIL-2/CD25 and anti-PD-1 experiments in Fig 7A. (**B**) Tumor growth is shown for the S4B6-IL2/IC and anti-PD-1 experiment in Fig 7C.

Supplementary Table 1. List of fluorochrome-labeled, biotin-labeled monoclonal antibodies, and fluorochrome-streptavidin conjugates used for flow cytometry in this study, along with source and staining concentration.

Antigen	Clone	Fluorophore	Concentration	Company	Cat. No.
CD45.2	104	APC	1:100	BioLegend	109814
CD45.2	104	APC-Cy7	1:100	Invitrogen	10-0454-81
CD45.2	104	Biotin	1:100	BD Biosciences	558702
CD3	17A2	AlexaFluor700	1:100	Invitrogen	56-0032-82
CD3	17A2	BV750	1:100	BioLegend	100249
CD3	145-2C11	FITC	1:150	Invitrogen	11-0031-82
CD4	RM4-5	BV510	1:100	BioLegend	100553
CD8α	53-6.7	Alexa Fluor 700	1:100	Invitrogen	56-0081-82
CD8α	53-6.7	BV605	1:100	BioLegend	100744
CD8α	53-6.7	BV650	1:100	BioLegend	100742
CD8α	KT15	FITC	1:100	Invitrogen	MA5-16759
CD8α	53-6.7	PerCP-Cy5.5	1:100	BioLegend	100734
CD44	IM7	Pacific Blue	1:50	BioLegend	103020
CD44	IM7	PE	1:300	Invitrogen	12-0441-83
CD44	IM7	Alexa Fluor 700	1:100	BioLegend	103026
CD44	IM7	APC-Cy7	1:100	BioLegend	103028
CD25	PC61	BV605	1:100	BioLegend	103036
CD25	3C7	PE	1:100	BioLegend	101904

CD25	PC61	PE-Cy7	1:100	BioLegend	102016
CD25	PC61	PE-Texas Red	1:100	BioLegend	102048
CD11b	M1/70	FITC	1:100	Invitrogen	11-0112-41
CD11b	M1/70	BV650	1:100	BioLegend	101259
CD11c	N418	BV605	1:100	BioLegend	117333
CD19	ID3	BV711	1:200	BD Biosciences	563157
CD19	6D5	PE/Dazzle 594	1:200	BioLegend	115554
CD49b	DX5	PE-Cy7	1:50	BioLegend	108922
Ly6C	AL-21	Biotin	1:500	BD Biosciences	557359
Ly6G	1A8	APC-Cy7	1:100	BioLegend	127624
Gr-1	RB6-8C5	FITC	1:100	BioLegend	108406
MHC CII (I-A/I-E)	M5/114.15.2	PerCP-Cy5.5	1:200	BioLegend	107626
NK1.1	PK136	PE	1:100	BioLegend	108708
PD-1 (CD279)	J43	BV421	1:50	BD Biosciences	565942
PD-1 (CD279)	RMP1-14	PE	1:100	BioLegend	114118
PD-1 (CD279)	RMP1-30	Biotin	1:100	BioLegend	109106
LAG-3 (CD223)	C9B7W	PerCP-Cy5.5	1:40	BD Biosciences	564673
Streptavidin	N/A	BV605	1:100	BioLegend	405229
Streptavidin	N/A	PE-CF594	1:100	BD Biosciences	562284
Streptavidin	N/A	PE-Cy7	1:100	Invitrogen	25-4317-82

Foxp3	FJK-16s	eFluor 450	1:200	Invitrogen	48-5773-82
Foxp3	FJK-16s	PerCP-Cy5.5	1:100	Invitrogen	45-5773-82
Foxp3	FJK-16s	PE-Cy7	1:100	Invitrogen	25-5773-82
Foxp3	FJK-16s	Alexa Fluor 488	1:100	Invitrogen	53-5773-82
Ki67	B56	Alexa Fluor 700	1:50	BD Biosciences	561277
TOX	TXRX10	eFluor 660	1:40	Invitrogen	50-6502-82
TCF1	S33-966	PE	1:50	BD Biosciences	564217
Granzyme B	GB11	Alexa Fluor 647	1:50	BD Biosciences	560212
TNFα	MP6-XT22	PerCP-Cy5.5	1:100	BioLegend	506322
IL-2	JES6-5H4	PE-Cy7	1:20	Invitrogen	25-7021-82
IL-2	JES6-5H4	PE	1:100	BioLegend	503808
IFNγ	XMG1.2	PE/Dazzle 594	1:100	BioLegend	505846
Fixable Viability Dye	N/A	eFluor 455UV	1:100	Invitrogen	65-0868-18
Fixable Viability Stain	N/A	440UV	1:100	BD Biosciences	566332
AH1 Tet	N/A	APC	1:150	N/A	N/A
AH1 Tet	N/A	BV421	1:150	N/A	N/A
Neg control Tet	N/A	PE	1:150	N/A	N/A